Tr. J. of Physics
23 (1999) , 399 – 413.

International Workshop:
"Magnetic Activity in Cool Stars"
(ed. O. Demircan)

Magnetic Activity in the Extreme Ultraviolet

Mihalis MATHIOUDAKIS
Department of Pure and Applied Physics
Queens University of Belfast, Belfast BT7 1NN, Northern Ireland

Received 18 July 1998

Abstract

The wealth of astronomical observations obtained in the extreme ultraviolet in recent years, have allowed comprehensive studies of the stellar transition regions and coronae to be carried out. For the first time we have been able to resolve individual coronal lines of various elements formed over a large temperature range (10^5 – $10^{7.2}$ K). The temperature, densities, abundances and magnetic field strengths of the stellar coronae can now be determined. Here we review some of the observations in the field of cool stars and discuss the implications on atmospheric heating requirements.

1. Introduction

The occurrence of convective envelopes in F, G, K and M stars is closely related with the existence of high temperature regions in the atmosphere. As the Sun is a dwarf G star, the study of late-type stars allows us to put the evolution of stellar and solar activity in prospective. The non-radiative heating processes originate in the convection zone. The convection zone has a two fold influence on atmospheric heating. Firstly, through its interaction with rotation resulting in the dynamo action and secondly by the generation of acoustic waves from the turbulent motions. It is the magnetically heated processes that are of the most importance in the vast majority of late-type stars. The temperature stratification in the atmosphere is determined by the amount of energy transported through the atmosphere. If there is only radiative energy taken in and out of a certain layer, we would have radiative equilibrium. This means that the amount of energy coming from the lower atmosphere, provides only enough energy to keep the upper atmosphere to a lower temperature. Since we observe the upper atmosphere to be hotter than the photosphere, some kind of non-radiative heating is required. One of the methods for determining the temperature structure of the Sun and other stars is the semi-empirical modelling of spectral lines [1],[2]. The negative temperature gradient in the photosphere (5,800 – 4,500 K), is followed by a temperature rise in the chromosphere (6,000 – 10,000

K), a very steep rise through the transition region so that the corona reaches temperatures in excess of 10^6 K. As a result of the high temperatures, the transition region and coronae contain a large number of highly ionized species emitting primarily in the ultraviolet (UV), extreme ultraviolet (EUV) and X-rays. With the large number of dedicated missions such as IUE, EINSTEIN and EXOSAT in the 1970's and 1980's, the field of UV and X-ray astronomy saw several major breakthroughs. In the early 1990's the Extreme Ultraviolet Explorer (EUVE) satellite and the Wide Field Camera (WFC) which was flown as part of the ROSAT mission, allowed us to fully explore the EUV sky.

The major difficulty with observations in the EUV lies with the absorption of light as it travels through the interstellar medium. The sources of attenuation between 60 – 912Å are hydrogen (H I), helium (He I) and ionized helium (He II). Hydrogen is the most abundant element and in the cool interstellar space the vast majority of H I atoms are in the ground state. The bound-free absorption coefficient per hydrogen atom σ_{bf} as a function of wavelength λ is given by

$$\sigma_{bf} \, = \, 1.05 \, \times \, 10^{-26} \lambda^3 \tag{1}$$

where σ_{bf} is measured in cm^2 and $\lambda \leq 912$Å in Å. He I starts to absorb at $\lambda \leq 504$Å where for $\lambda \leq 228$Å He II is added to the sources of opacity. The attenuated intensity $I_\lambda(s)$ is given by

$$I_\lambda(s) \, = \, I_\lambda(0) e^{-\tau_\lambda(s)} \tag{2}$$

where $I_\lambda(0)$ is the unattenuated intensity and $\tau_\lambda(s)$ the optical depth. The optical depth is the sum of all the parameters that contribute to the attenuation

$$\tau_\lambda \, = \, \sigma_{HI} N_{HI} \, + \, \sigma_{HeI} N_{HeI} \, + \, \sigma_{HeII} N_{HeII} \tag{3}$$

where σ are the H I, He I and He II cross sections and N the corresponding interstellar column densities. The interstellar medium transmission as a function of wavelength for a hydrogen column density of $\mathrm{N}_H \, = \, 10^{18}$ atoms per cm^{-2} is given in Fig. 1. It has been derived using the latest hydrogen, helium and ionized helium cross-sections [3].

In this paper we will provide a brief description of the EUVE mission and objectives, followed by techniques used in the analysis and interpretation of the observations. An outline of some of the results in the field of cool stars will also be presented.

2. The EUVE mission

The Extreme Ultraviolet Explorer (EUVE) is a NASA mission which was launched into a near-Earth orbit from Cape Canaveral on June 7 1992. The mission had the following primary scientific objectives.

- To carry out an all-sky survey in four passbands covering the wavelength ranges 60–200Å(Lex/B), 160–240Å(Al/Ti/C), 345–605Å(Ti/Sb/Al) and 500–740Å(Sn/SiO).

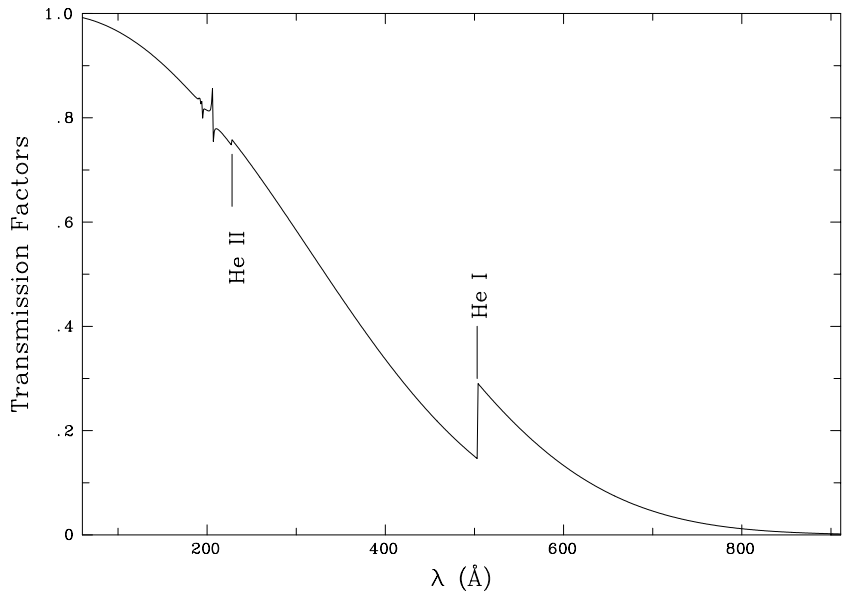

Figure 1. The interstellar medium transmission factors for a hydrogen column density of $N_H = 10^{18}$ atoms per cm^{-2} and abundance ratios of $\frac{HeI}{HI} = 0.09$ and $\frac{HeII}{HI} = 0.01$.

- To conduct a deep survey (DS) in a $2^o \times 180^o$ strip of the sky along the ecliptic equator in the Lex/B (60–200Å) and Al/C (170–360Å) bands. The DS is about a factor of 20 more sensitive than the all-sky survey.
- To perform pointed spectroscopic observations with a resolution of $\frac{\lambda}{\Delta\lambda} \sim 150 - 350$ over the 60−740Å wavelength range.

The science payload onboard EUVE comprises of four grazing-incidence Walter-Schwarzschild telescopes. Three of the telescopes are co-aligned and point at right angles to the satellite spin axis. The fourth telescopes is co-aligned with the satellite spin axis and is divided into six equal segments. Three of the segments provide light for the DS photometric instrument while the other three provide light for the spectrometers. Each EUVE orbit lasts for ≈ 90min and useful data are collected only during orbital night ≈ 30min. In the all-sky survey observing mode, the DS was pointing in the ecliptic equator while the spacecraft rotated around the spin axis three times per orbit; in this way the three all-sky survey telescopes were covering a full circle in the sky. The DS telescope while pointing in the anti-Sun direction advanced by 1^o per day along the ecliptic equator so that the survey instruments covered the whole sky in six months. The all-sky coverage varied as a function of ecliptic latitude with sources in the ecliptic equator being scanned for a minimum of 5 days while sources at the poles were scanned throughout the six month survey [4].

3. Broad band EUV photometry

The sources detected during the all-sky survey include late-type stars, white dwarfs, cataclysmic variables, extragalactic objects, A, B stars and several unidentified sources [5]. The strong attenuation of light in the EUV limits the observational sample to nearby objects. Late-type stars constitute over 50% of the detected sources therefore allowing statistical studies of their EUV properties to be carried out. In a recent paper [6] a group of single main sequence dwarfs was selected, with spectral types ranging from mid F to late M and the EUV rotation-activity relation was examined. It was shown that the ratio of rotational period to convective overturn time, i.e Rossby number (R_O), is a better parameter for describing the EUV levels of activity as compared to the rotational period alone. As more surface field is generated with increased rotation and deep convection, the heating mechanism and consequently the radiative emission reaches a maximum (i.e. saturation). This is evident in Fig. 2(b) where we see that the Mg II emission begins to level off at low R_O numbers. A comparison of the coronal emission in the Lex/B band with the Mg II chromospheric emission shows that saturation in the EUV occurs in lower Rossby numbers than chromospheric emission (Fig 2(a)(b)). In other words, chromospheric saturation is reached at lower rotation rates than coronal saturation. It is evident that at any given value of the Rossby number, the scatter in the Lex/B diagram is significantly higher than in Mg II. We know from the solar case that there is a factor of ten variation in the integrated coronal X-ray emission during the solar cycle whereas the chromospheric emission varies only by about a factor of two. Since the EUVE all-sky survey observations are essentially an snapshot of the EUV sky, (they were taken over a six month period), some of the objects were observed in their equivalent solar maximum while others were observed in their minimum.

The studies of rotational modulation in late-type stars provide information of the distribution of active regions on the stellar surface. The RS CVn binary HR 1099 was observed both during the all-sky survey and during a continuous pointing calibration observation in the EUVE Lex/B band. Both observations covered more than the 2.86 day rotational period of the system and showed strong evidence for rotational modulation in the coronal emission of this source [7].

A spectacular flare event with a total energy in excess of 10^{35} ergs was observed on the dM2.5e star AU Mic [8]. The flare consisted of a sharp impulsive peak lasting for 2 hours followed by a decaying tail which lasted for about 1 day. If we assume that no energy input occurs during the event, one would expect the flare plasma to cool mainly by radiation and conduction. The radiative and conductive cooling timescales are given by

$$\tau_{rad} = \frac{3\,k\,T_e\,V}{n_e \Lambda(T_e)} \tag{4}$$

$$\tau_{cond} = \frac{3\,n_e\,k\,L^2}{V\,c\,T_e^{5/2}} \tag{5}$$

where k is Boltzmann's constant, T_e the temperature, V the volume of the emitting

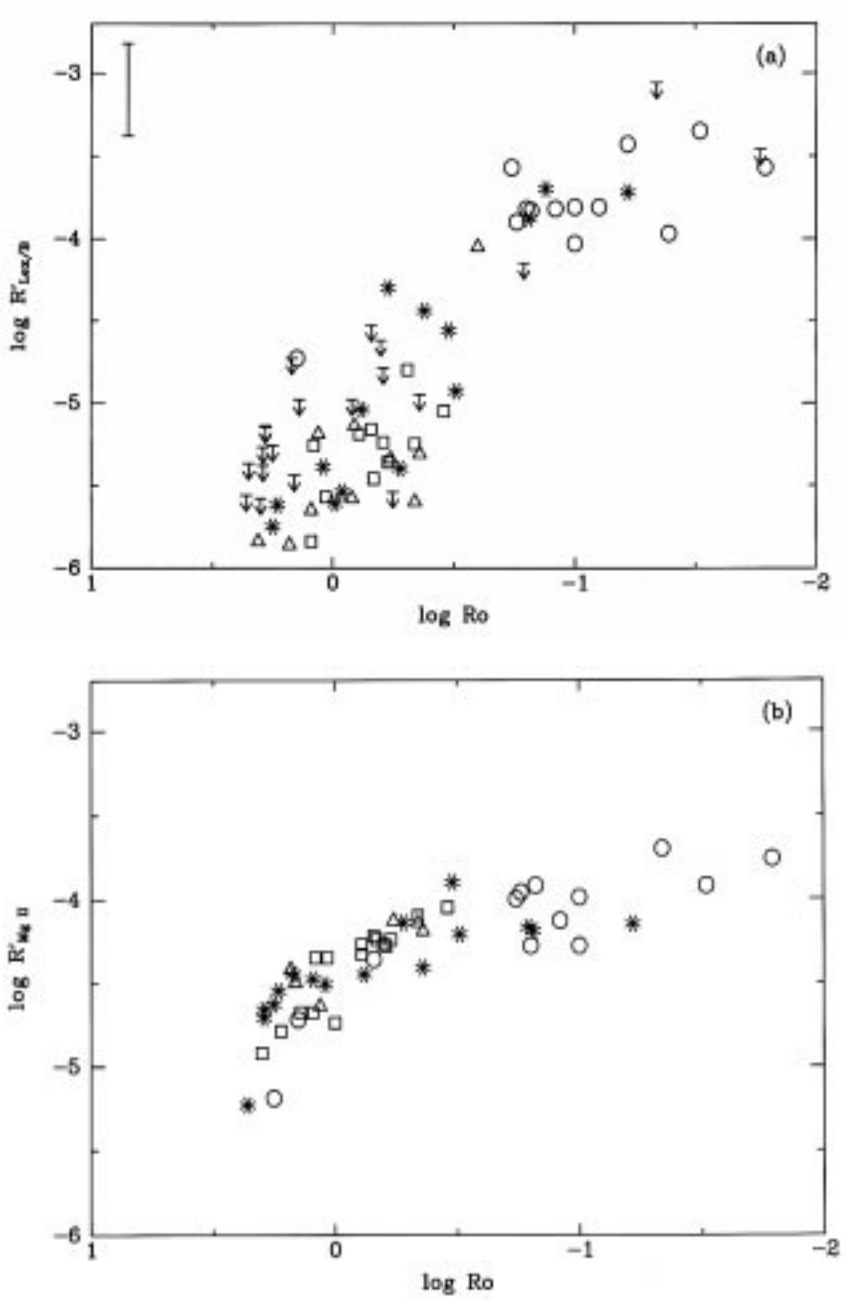

Figure 2. The Rossby number as a function (a)$R'_{Lex/B}$ and (b)R'_{MgII}, where R′ is the luminosity in these bands normalized to the bolometric luminosity. The symbols correspond to △ dF, □ dG, ∗ dK and ◯ dM stars.

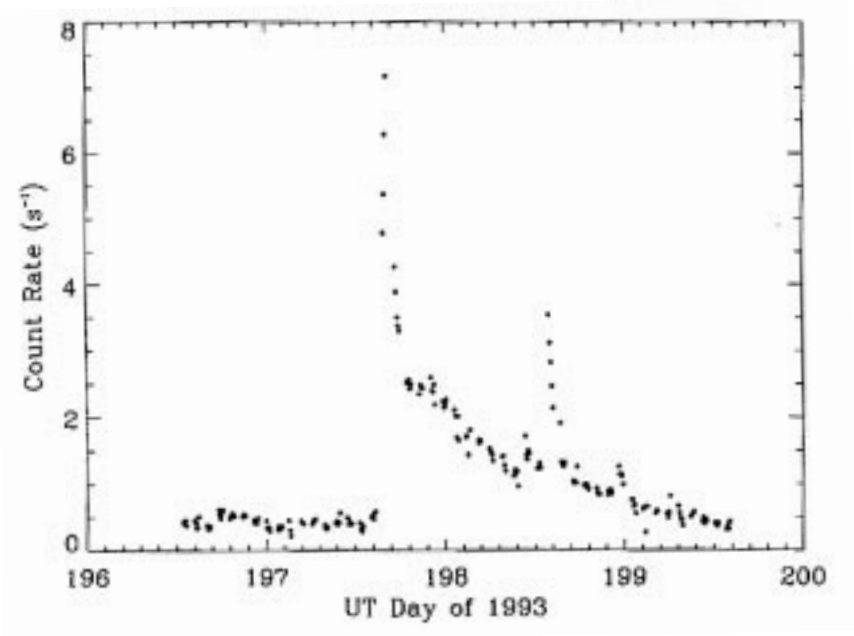

Figure 3. The EUVE Lex/B lightcurve of the AU Mic flare (reproduced from [8]).

plasma, n_e the electron density, $\Lambda(T_e)$ the radiative loss function, L the loop half length and c a constant [9]. The observed timescale of the AU Mic event are much longer than the radiative and conductive timescales. It has been shown that the long decay phase of the event can only be explained by a model of rapid expansion, where the plasma becomes tenuous sufficiently quickly to avoid catastrophic radiative cooling [8]. However, this model and indeed the vast majority of models do not include any heating during the decay phase of the flare. It remains to be investigated whether the long lightcurve can be interpreted with a model where the dominant cooling processes are radiation and/or conduction, with continual heating taking place throughout the duration of the event. This is known to take place in the solar two-ribbon flares where each newly formed loop may cool quite rapidly, but the continual formation of new loops gives the appearance of a very long lived event [10].

4. Stellar Coronal Spectroscopy

The greatest capability of EUVE is through its spectroscopy which allows the observation of individual coronal lines formed in the 10^5 to $10^{7.2}$ K temperature range. The line to continuum ratios, radiative losses, elemental abundances, electron densities can now be determined. An assessment of the atomic data in this relatively unexplored region of the electromagnetic spectrum can also be carried out. To date, high signal-to-noise EUV

spectra have been obtained for a large number of sources with sample spectra presented in Fig. 4. Procyon is a low activity F subgiant and its spectrum is dominated by the lower ionization stages of iron (Fe IX – Fe XVI) indicating a maximum coronal temperature of $10^{6.2}$ K. The EUV spectrum of the active RS CVn binary σ Crb is dominated by Fe XV - Fe XXIV therefore indicating coronal temperatures in excess of $10^{7.2}$ K. Procyon is an example of a *cool* corona whereas σ Crb is a *hot* coronal source. We emphasize that Fe XXIV is the highest ionization stage of Fe detected in the EUV range; it is therefore likely that σ Crb has a significant amount of material at even higher temperatures. The EUVE spectral atlas compiles the spectra of the brightest sources [11].

In this section we will outline the main principles regarding the flux of a coronal line followed by some of the results from various spectroscopic studies.

4.1. The flux of a coronal line

The plasma in the transition region and corona is collisionally dominated. In the case of an atom with an upper level u and a lower level l the observed line flux F_{ul} is given by:

$$F_{ul} = \frac{h\nu_{ul}A_{ul}}{4\pi r^2}\int_{\Delta V}\frac{n_u}{n_{ion}}\frac{n_{ion}}{n_{el}}A_{el}\frac{n_H}{n_e}n_e dV. \quad (6)$$

where $\frac{n_u}{n_{ion}}$ is the population of level u relative to the ion; $\frac{n_{ion}}{n_{el}}$ is the relative population of the ion; $\frac{n_{el}}{n_H} = A_{el}$ is the abundance of the element relative to hydrogen; $\frac{n_H}{n_e} = 0.8$ is the number density of hydrogen relative to the number density of the electrons and n_e is the number density of the electrons. For emission lines such as the resonance lines of Li-like ions, only the ground level (l=1) and the excited level (u=2) of the line are important for calculating the line flux. In most cases collisional de-excitations are not important and since the radiation field is very low, we can assume that the collisional excitations from the ground level are balanced by spontaneous radiative decays from the excited level i.e.:

$$n_e n_l C_{lu} = n_u A_{ul} \quad (7)$$

where A_{ul} is the Einstein coefficient and C_{lu} is the collision probability or collision rate coefficient [12].

The collision rate coefficient is given by

$$C_{lu} = \frac{8.63\times10^{-6}}{g_l kT^{3/2}}\int_{E_{lu}}^{\infty}\Omega_{lu}e^{-\frac{E}{kT}}dE \quad (8)$$

where Ω_{lu} is the collision strength, g_l the statistical weight of the lower level and $E_{lu} = h\nu_{lu} = h\nu_{ul}$ is the minimum energy required for the transition. Equation (6) for the line flux then becomes :

$$F_{ul} = \frac{8.63\times10^{-6}h\nu_{ul}0.8\,A_{el}\Omega_{lu}}{4\pi r^2 g_l}G(T)EM. \quad (9)$$

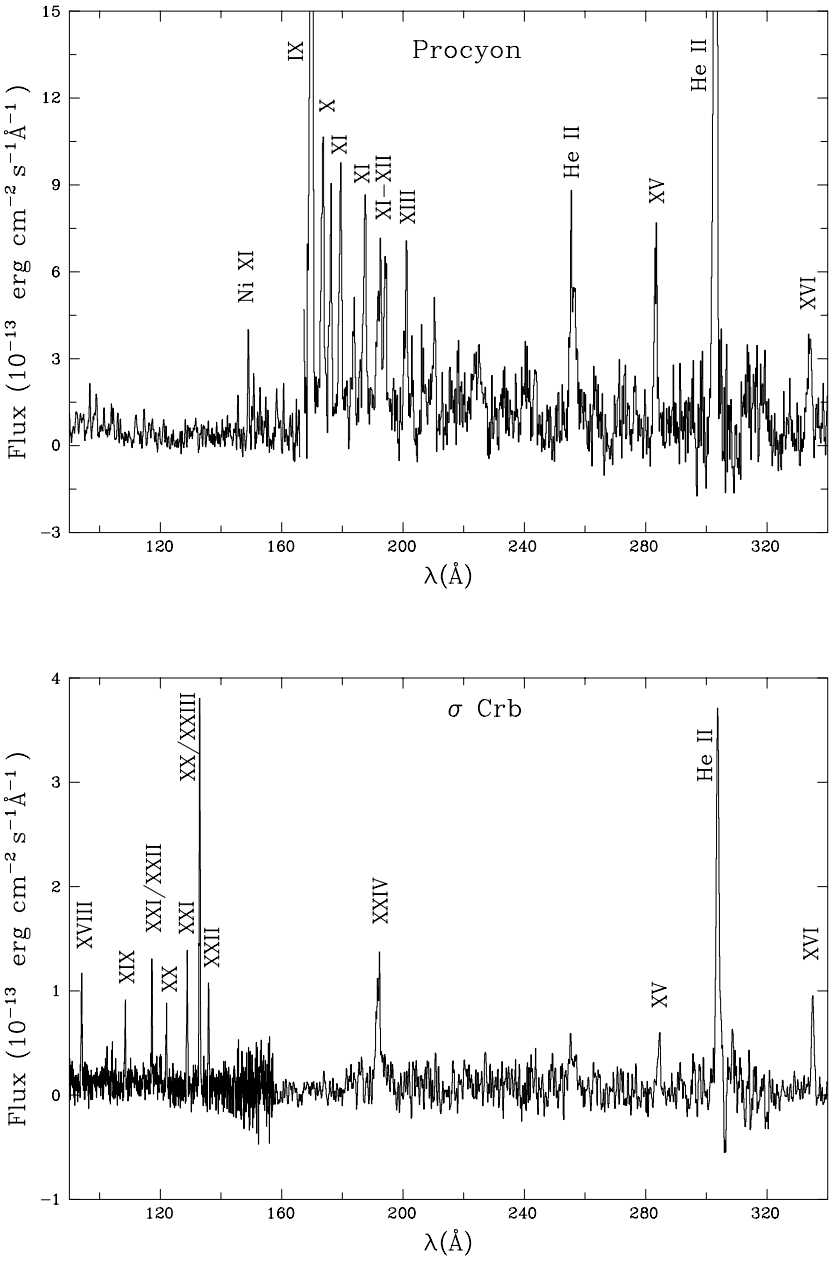

Figure 4. Sample EUV spectra of late-type stars. Procyon is a typical example of a *cool* corona whereas σ Crb is a *hot* coronal source. The strongest Fe lines are indicated by their ionization stage.

where $G(T)$ is the line contribution function and EM the emission measure.

$$G(T) = \frac{n_{ion}}{n_{el}} T^{-1/2} e^{\frac{-h\nu_{ul}}{kT}} \tag{10}$$

$$EM = \int_{\Delta V} n_e^2 dV \tag{11}$$

The atomic parameters of a transition, i.e. collision strengths and statistical weights, can be calculated; the line flux can be measured from observations. If we know the abundance of the element and the ionization balance, equation (9) becomes very useful as it provides a single value for the emission measure at the peak temperature of line formation. The physical meaning of the emission measure is that, it denotes the amount of material over a certain volume and as a result the emitting power over a specific temperature range contained in that volume.

4.2. The emission measure distribution

The collision rates, elemental abundances and ionization balance are often combined into one quantity called *The line emissivity*. The volume emission measure can be described with the simplified relation

$$EM(T) = 4\pi d^2 \frac{F_{obs}}{\epsilon} \tag{12}$$

where d is the distance to the object, F_{obs} the observed flux and ϵ the corresponding line emissivity. Using this relation the emission measure of each individual spectral line can be calculated and the distribution of emission measures as a function of temperatures can be derived. The emission measure distribution (EMD) of HR 1099 is shown in Fig. 5. A number of attempts have been made to interpret the EMD in terms of loop geometry. The temperature and density distribution in a loop is determined by the energy balance equation

$$E_H + E_R - \nabla \cdot \mathbf{F_C} = 0 \tag{13}$$

where E_H is the mechanical energy input, E_R is the term describing the radiative losses and F_C the conductive heat flux along the magnetic field. Additional factors include the variation in the cross-section of the loop and hydrostatic equilibrium. The steady state energetics of simple models of coronal loops have been considered by [13]. In these models, mass flows are negligible and drifts of material across the field lines are also neglected. The magnetic pressure dominates over the gas pressure so that heat conduction occurs along the field lines. These assumptions reduce the dimensionality of the problem. Simple physical considerations require that hydrostatic solution are stable only if the maximum temperature T_{max} is located at the apex of the loop. The following scaling law was found [13], between T_{max}, the loop half length (L) and pressure p

$$T_{max} = 1400\,(pL)^{1/3}. \tag{14}$$

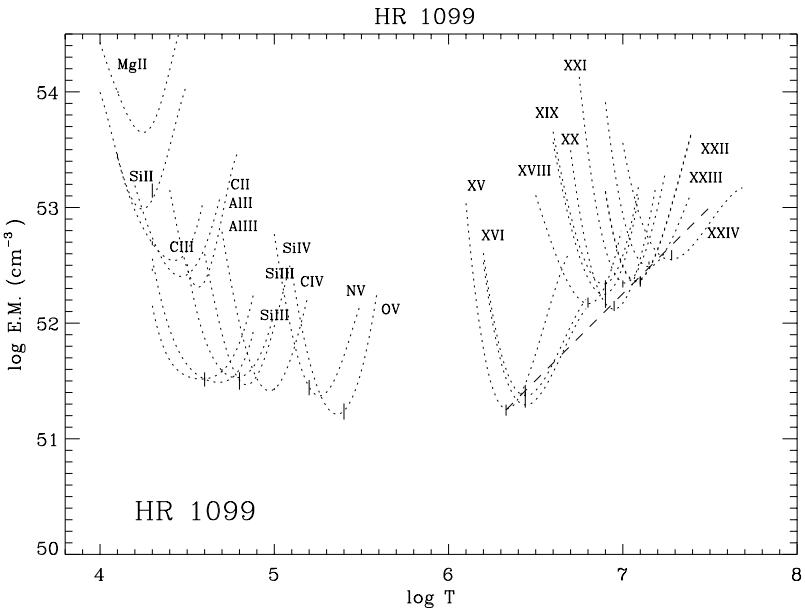

Figure 5. The emission measure distribution of HR 1099. The line contribution functions are plotted as dotted lines whereas the $T_e^{1.5}$ dependence at high temperatures is shown as a dashed line. The lines at temperatures below $10^{5.3}$ K have been determined from IUE SWP spectra.

A detailed comparison of EMDs derived from quasi-static coronal loop models, with the EMDs derived from EUVE spectroscopic observations has been carried out [14]. The EMD of a coronal loop peaks at the maximum temperature of the loop (T_{max}) and the emitted spectrum is dominated by emission lines formed at that temperature. However, it is the gradual tail of the EMD that provides information on the thermodynamic structure of the loop. The complexity seen in the high temperature part of the EMDs of RS CVn binaries with a local peak at log T_e= 6.8 – 6.9 and a maximum emission measure at log T_e = 7.2 [15], requires at least two populations of coronal loops with apex temperatures constrained by the two maxima.

4.3. Assessing the atomic data

Coronal plasma conditions are encountered rarely, if ever, in terrestrial laboratories. Coronal observations often provide the only means of assessing the reliability of atomic data for a large number of transitions. In the previous section we have shown how the collision strength and statistical weight enter the equation for the line flux. The EMD can be used to test the reliability of atomic data for a large number of transitions. In order to use this technique our starting point is the observed spectrum of a source where we select a set of strong lines covering a broad range of temperatures; based on these lines we derive the EMD. We then use equation (9) to follow the opposite procedure that is, we

input the derived EMD and the atomic data from a complete line list normally containing hundreds of lines. The predicted flux for **all** the lines in the list that are formed over that temperature range can therefore be derived. An example is shown in Fig 6. The strongest lines in the EUV spectra of HR 1099 have been used to construct the emission measure distribution (Fig 5). The emission measure distribution was then combined with the line emissivity lists of [16] to produce synthetic spectra (Fig 6b). As is evident the very strong Fe XX line at 126.53Å is not detected in the observed spectrum. The discrepancy between the observed and predicted spectrum can not be due to incorrect abundances or ionization balance as the remaining lines of Fe and Fe XX in particular, are in good agreement with the observations. The error was found in the collision rate coefficients and was later rectified [17].

4.4. Coronal Density Diagnostics

In the vast majority of coronal lines the excited levels are populated by collisional excitation and depopulated by spontaneous radiative decays. These are the so called *allowed* transitions. However, some levels exists where the transition probability is quite small; these are the *intercombination* and *forbidden* transitions. If an ion has one level populated by collisions and depopulated by spontaneous radiative decays and a second level that is populated by collisions and depopulated by both collisions and spontaneous radiative decays, then the ratio of the two lines is density sensitive [12]. The EUV spectral range offers several line ratios that can be used as density diagnostics [18]. In the case of Procyon and α Cen, [19] and [20] have used Fe IX - Fe XVI line ratios to derive coronal densities in the range of 10^9 to 10^{10} cm^{-3}. In *hot* coronal sources, Fe XXI line ratios are widely used as they provide good diagnostic for high density plasmas ($10^{11.5}$ – 10^{15} cm^{-3}). The Fe XXI line ratios applicable in most cases are R_1=(102.22Å/128.73Å), R_2=(121.22Å)/(128.73Å) and R_3=(142.15Å)/128.73Å). These line ratios were applied to the active F dwarf HR 1817 and allowed us to derive an upper limit of $n_e \leq 10^{11.7}$ cm^{-3} to the electron density [21]. The electron density combined with the emission measure led us to conclude that the volume of the emitting plasma should be greater than 2×10^{28} cm^3. If we assume that the coronal plasma is distributed in semicircular loops with cross-sectional diameters $\approx$ 20% of the footpoint separation, the radius of the loop is given by

$$R \geq 3.7 \times 10^9 n^{-\frac{1}{3}} \tag{15}$$

where n is the number of loops and R is measured in cm. With an upper limit to the density we can derive an upper limit for the pressure of $p \leq 10^3$ dyne cm^{-2} at the temperature of 10^7 K. The confinement of the gas therefore requires a magnetic field of B$\leq$160 Gauss. There are some indications that very high densities, $\sim 10^{12}$ – 10^{13}, cm^{-3} exist in the corona of some RS CVn binaries [22]. If coronal densities of 10^{13} cm^{-3} are indeed confirmed, they will imply very small volumes with intense coronal heating and magnetic fields of several hundred Gauss. Assuming that the coronal heating energy is dissipated by the magnetic field, a simple comparison of the radiative and dissipation

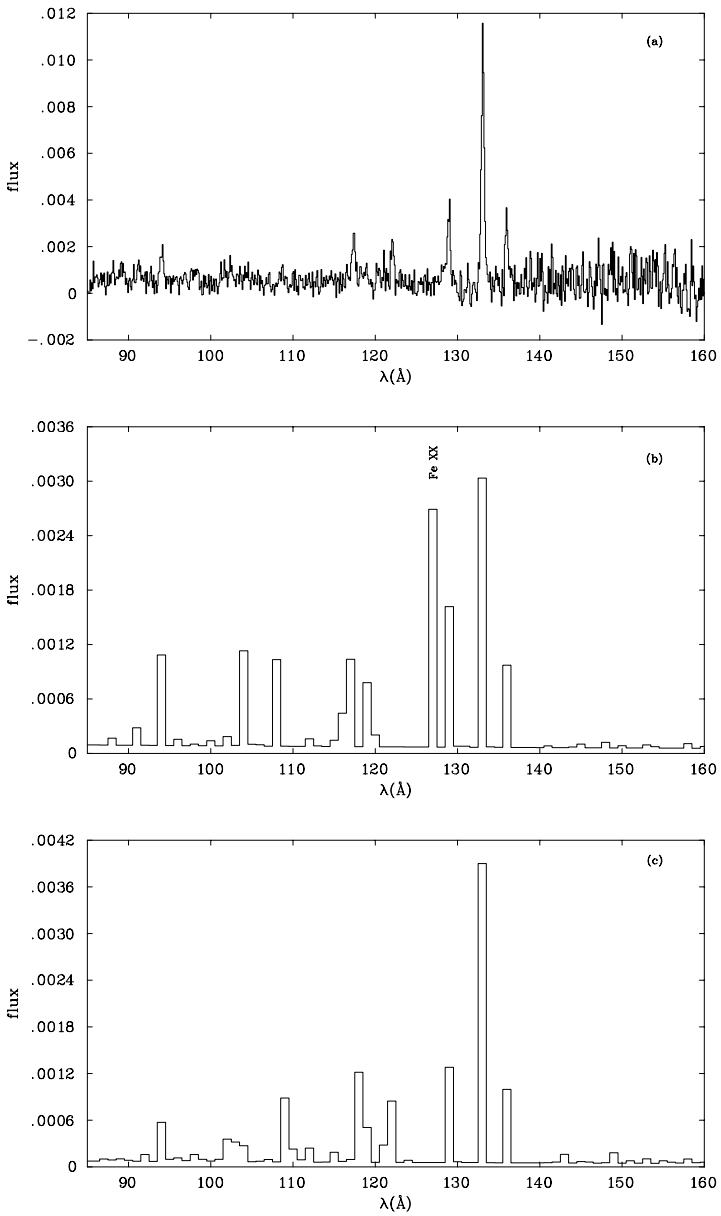

Figure 6. (a) The observed short wavelength spectrum of the RS CVn binary HR 1099 and the synthetic spectra derived using (b) the Landini & Monsignori-Fossi (1990) and (c) the Mewe et al. (1997) line emissivities. The fluxes are in relative units. The Fe XX 126.53Å line is noted. The difference in the flux values between the observed and synthetic spectra is due to different binning in the wavelength scale.

timescales shows that the lifetime of the loops is of the order of a few seconds [14]. If that is the case, the quasi-static loop assumption can no longer hold.

4.5. Stellar coronal abundances

In the solar corona elements with a low first ionization potential (FIP) (e.g. Si, Mg, Fe) appear to be enhanced relative to elements with a high FIP (e.g. O, Ne) [23]. A thorough investigation of this effect in stars has been carried out in a series of papers by J. Drake and collaborators. The method used is based on a comparison of a "baseline" EMD with the emission measure derived from individual elements. The technique was applied successfully in several objects including Procyon, α Cen, ϵ Eri (see [24] and references therein). No evidence for a solar like FIP effect was found on Procyon; this was attributed to that the coronal and transition region emission may originate in low-altitude structures similar to the solar supergranulation network [25]. In the remaining objects the results are still not conclusive.

One of the best pronounced features in the EUV spectra of late-type stars is an "excess" flux or continuum emission in the wavelength range of 70 - 120Å(see Fig 4). The continuum was originally attributed to opacity effects [26]. The idea is based on that strong coronal lines, i.e. those with high oscillator strengths, can have high optical depths. If the emitting plasma lies below a scattering region an assymetry is created where more photons are scattered down than up. The net effect is that strong lines appear weaker relative to the continuum and the weak lines. This interpretation has received strong criticism by [27] who find it to be inconsistent with the ROSAT PSPC observations. Alternatively, the continuum could be produced by free-free emission from large amounts of plasma with temperatures in excess of $10^{7.4}$ K. However, the values predicted for the emission measure at these temperatures do not reproduce the EXOSAT, GINGA and ASCA observations. The most convincing explanation for the reduced line-to continuum ratio has been offered by [28] who suggest that iron is underabundant in the corona of Algol by as much as 20% of the solar photospheric value. A more extreme case is that of CF Tuc with metal abundances 10 times below the solar value [29]. In fact several active stars and RS CVn binaries [30] appear with coronal abundance deficiencies, to the extend that is could be suggested that it is the Sun that appears to have exceptionally high metal abundances!!

The new abundances have important implications on the radiative output of the corona. The radiative losses are computed as the product of the emission measure with the radiative loss function $\Lambda(T_e)$ of an optically thin plasma [31]. Iron becomes an increasingly important contributor to the $\Lambda(T_e)$ for temperatures above 10^5 K and dominates between $10^{5.7}$ – $10^{6.5}$ K. A reduced Fe abundance will increase the emission measure (see eq. 9) and decrease $\Lambda(T_e)$, causing little difference in the radiative losses in the temperature range where $\Lambda(T_e)$ is dominated by Fe. However, a significant increase in the radiative losses is found at temperatures above $10^{6.5}$ K where Fe is no longer the dominant cooling agent. In higher temperatures radiative losses from bremsstrahlung radiation become important [21]. The radiative losses provide a lower limit to the coronal

heating requirements; therefore the new Fe abundances need to be taken into account when considering the energy balance of the corona.

References

[1] Vernazza J.E., Avrett E.H., Loeser R., ApJS 31 (1976) 1.

[2] Houdebine E.R., Doyle J.G., A&A 289 (1994) 169.

[3] Rumph T., Bowyer S., Vennes S., AJ 107 (1994) 2108.

[4] Haisch B., Bowyer S., Malina R.F., JBIS 46 (1993) 331.

[5] Bowyer S., Lampton M., Lewis J., Wu X., Jelinsky P., Malina R.F., ApJS 102 (1996) 129.

[6] Mathioudakis M., Fruscione A., Drake J.J., McDonald S., Bowyer S. & Malina R.F., A&A 300 (1995) 775.

[7] Drake J., Brown A., Patterer R.J., Vedder P.W., Bowyer S., Guinan E.F., ApJ 421 (1994) L43.

[8] Cully S.L., Fisher G.H., Abbott M.J., Siegmund H.W., ApJ 435 (1994) 449.

[9] Spitzer L., Physics of Fully Ionized Gases, Interscience, New York.

[10] Cargill P.J., Priest E.R., ApJ 266 (1983) 383.

[11] Craig N., Abbott M.J., Finley D., Jessop H., Howell S.B., Mathioudakis M., Sommers J., Vallerga J.V., Malina R.F., ApJS 113 (1997), 131.

[12] Mariska J.T., The Solar Transition Region, (Cambridge University Press, 1992).

[13] Rosner, R., Tucker, W.H., Vaiana, G.S., ApJ 220 (1978), 643

[14] van den Oord, G.H.J., Schrijver, C.J., Camphens, M., Mewe, R., Kaastra, J.S., A&A 326 (1997), 1090.

[15] Griffiths N.W., Jordan C., ApJ 497 (1998), 883

[16] Landini M., Monsignori-Fossi B.C., 1990, A&AS 82, 229.

[17] Mewe, R., Kastra, J.S., van den Oord, G.H.J., Vink, J., Tawara, Y., A&A 320 (1997), 147

[18] Keenan F.P., Space Sci Rev 75 (1996), 537.

[19] Schmitt J.H.M.M., Drake J.J., Haisch B.H., Stern R.A., ApJ 467 (1996), 841.

[20] Foster V.J., Mathioudakis M., Keenan F.P., Drake J.J., Widing K.G., ApJ 473 (1996), 560

[21] Mathioudakis M., Mullan D.J., A&A, (1998), submitted.

[22] Dupree A.K., Brickhouse N.S., Doschek G.A., Green J.C., Raymond J.C., ApJ 418 (1993), L41

[23] Laming J.M., Drake J.J., Widing K.G., ApJ 443 (1995), 416.

[24] Drake J.J., In the 9th Cambridge Workshop on Cool Stars Stellar Systems and the Sun, eds. R. Pallavicini & A.K. Dupree, ASP Conference Series, vol. 109, p.203

[25] Drake J.J., Laming J.M., Widing K.G. ApJ 443, (1995), 393.

[26] Schrijver C.J., van den Oord G.H.J., Mewe R., A&A 289, (1994), L23.

[27] Schmitt J.H.M.M., Drake J.J., Stern R.A., ApJ 465, (1996), L51.

[28] Stern R.A., Lemen J.R., Schmitt J.H.M.M., Pye J.P., ApJ 444, (1995), L45.

[29] Schmitt J.H.M.M., Stern R.A., Drake J.J., Kurster M., ApJ 464, (1996), 898.

[30] Tagliaferri G., Covino S., Fleming T.A., Gagne M., Pallavicini R., Haardt F, Uchida Y., A&A 321, (1997), 850.

[31] Cook J.W., Cheng C-C., Jacobs V.L., Antiochos S.K., ApJ 338, (1989), 1176.